NJC

Accepted Manuscript

ROYAL SOCIETY OF CHEMISTRY

www.rsc.org/njc

Core–shell cobalt oxide mesoporous silica based efficient electro-catalyst for oxygen evolution

Shahid Ali Khan[a,b], Sher Bahadar Khan[a,b]*, Abdullah M. Asiri[a,b]

[a]*Center of Excellence for Advanced Materials Research, King Abdulaziz University, Jeddah 21589, P.O. Box 80203, Saudi Arabia*
[b]*Chemistry Department, Faculty of Science, King Abdulaziz University, P. O. Box 80203, Jeddah 21589, Saudi Arabia*

* To whom correspondence should be addressed:

Dr. Sher Bahadar Khan; E-mail: sbkhan@kau.edu.sa; Tel: +966-593709796

Abstract

In the last few decades renewable resources got much attention for the production of hydrogen. Here in we present oxygen evolution from water by using cobalt oxide based nanomaterials (Co_3O_4, $Co_3O_4@SiO_2$, Co_3O_4/TiO_2, Co_3O_4/Fe_2O_3, $ZnO@SiO_2$). These nanomaterials were grown in a control size and characterized by various spectroscopic techniques. The Co_3O_4, $Co_3O_4@SiO_2$, Co_3O_4/TiO_2, Co_3O_4/Fe_2O_3, $ZnO@SiO_2$ were screened for their electro-catalytic properties in H_2O oxidation. All of these nanoparticles showed good oxygen evolution activity and high stability in alkaline conditions. However $Co_3O_4@SiO_2$ were showing a higher current density at lower over potential and lower Tafel slope (107.7 mV dec^{-1}) as compared to Co_3O_4/TiO_2, Co_3O_4/Fe_2O_3, $ZnO@SiO_2$, and Co_3O_4. At 1.0 V (overpotential 735 V versus Ag/AgCl) $Co_3O_4@SiO_2$ supplied a current density of 63.0 $mAcm^{-2}$ in 0.3M KOH solution. This indicated a superior electrocatalytic performance then the other electrocatalyst reported for oxygen evolution so far. This fascinating electrocatalytic performance of $Co_3O_4@SiO_2$ might be due to certain structural features, which elevate their electronic conductivity, oxidizing aptitude, and the affinity among OH ion and $Co_3O_4@SiO_2$ surface and ultimately enhance smooth mass transports which give superior oxygen evolution activity to $Co_3O_4@SiO_2$.

1. Introduction

Hydrogen is the main component of fuel cell and has much vital application in numerous important industrial processes. It could perform a vital role in the future hydrogen economy as an energy carrier. Currently energy crises, energy production and the environmental threats associated with it are the hot topic at the global level. The main challenging for present and future is the storage of fossil fuels and climatic change [1]. To cope these challenging it is very necessary to have a clean and benign environmental system for the energy production [2]. It seems that the need for energy might be double by the mid-century as compared to the present amount due to social development [3]. Some of the energy requirements will met by burning fossil fuels, but it severely deteriorates our climate [4, 5]. Due to the adverse effect of fossil fuels on environment, scientists divert their attention to convert solar energy to chemical energy by using hydrogen as a carrier of energy [6, 7]. With the invent of industrial revolution the CO_2 level raises in the past 800,000 years associated by an increase in the atmosphere temperature, the so called process known as greenhouse effect [8]. It was reported, that among the renewable resources of energy including geothermal, hydro power and wind energy, solar energy provide one of the largest quantity of energy to the earth surface [3]. But one of the main challenges for scientist how to capture and convert this solar energy to chemical energy. Therefore, electrochemical water oxidation provide one of the most promising and environmental benign method for the production of hydrogen [8].

A best electrocatalyst must have a low overpotential, and very close to Nernstian potential [9]. A number of cathodic materials were reported for the half reaction of H_2O/H_2 of water oxidation [10-13]. The catalytic activity of metal oxide was reported under different condition *i.e.* Mn_4OxCa for H_2O/O_2 half-reaction and nickel as an

anode under high temperature, pervoskite metal oxide under high alkaline solution and some transition metal oxide such as IrO_2, PtO_2, RuO_2, and Rh_2O_3, showing good activity in acidic medium for water oxidation [3]. To-date IrO_2 and RuO_2 catalyst are consider to be the best anode materials for OER production in water oxidation [14]. However their use is prohibited due to their high cost [4], scarce availability in earth crust and their less applicability at large scale [14], compel researcher for the search of benevolent alternative materials. Catalyst for oxygen evolution and reduction are the central theme for fuel cell and in renewable source technology. Although tremendous attempt were made for the development of oxygen evolving catalyst, however low cost and high catalytic performance is still a great challenge [16]. It was reported in literature that cobalt based nanomaterials play an important role in electrochemical water oxidation. An interesting anodic cobalt oxide oxygen evolving catalyst (Co-OEC) was produced in situ in an aqueous phosphate solution having Co^{+2} [9, 15]. The Co-OEC functions as a reference for oxygen evolving complex in photosystem II [17], in mild condition with overpotential of 420 mV and a self-healing catalyst [18]. Among the ORR cathodic material, Pt and its alloys play an important role in fuel cell. However due to the high cost of these precious metals, alternative catalyst were investigated as well as OER instead of ORR in energy storage and solar fuel cell [9, 10, 16]. The cobalt oxide grown on reduce mildly oxidize graphine oxide indicated a high performance in alkaline solution for ORR and OER catalytic activity [19].

In the current approach we selected different nanomaterials for water splitting and explored doping effect on the performance of cobalt oxide by doping with titanium oxide, iron oxide and silica. The silica core-shell over cobalt oxide exhibited excellent performance in OER. Further to assess the effect of silica on the water

oxidation performance, the $Co_3O_4@SiO_2$ was compared with $ZnO@SiO_2$ which suggested that silica is not responsible for high catalytic performance but the mesopourus nature of $Co_3O_4@SiO_2$ is important in water oxidation. The overpotential and current of the $Co_3O_4@SiO_2$ were measured at various concentration levels ranging from 0.1-0.3 M with a difference of 0.5 which indicate that overpotential is decreasing and current is increasing with increase in concentration of KOH solution.

2. Experimental

2.1. Materials

Different reagents such as cobalt(II) nitrate hexahydrate, nafion, ethanol, acetone, potassium hydroxide, and all other reagents were purchased from Sigma-Aldrich and used as such as received. All the solutions were prepared in deionized water, obtained from departmental Millipore-Q water purification system (18.2 MΩ.cm @ 25 ℃, TOC<10ppb).

2.2. Synthesis of nanomaterials

2.2.1. Synthesis of Co_3O_4

Salt of $Co(NO_3)_2 . 6H_2O$ (0.1 M) was dissolved in 100 mL deionized water and added 0.5 M of NaOH to the reaction mixture by raising the pH of the solution above 10, and stirred thoroughly for overnight at 60 ℃ followed by centrifugation. The supernatant liquid was withdrawn and the remaining solid part was washed thrice with deionized water and collected by centrifugation. At room temperature the surface of the particles was polished by removing the adsorbed unwanted materials and then drying the material by exposing in oven at 50 ℃.

2.2.2. Synthesis of core–shell cobalt oxide mesoporous silica microspheres ($Co_3O_4@SiO_2$)

$Co_3O_4@SiO_2$ microspheres were synthesized through a versatile solution sol–gel method [20] as follows. The above synthesized cobalt oxide nanoparticles (0.2 g) were added to a conical flask charged with water (20 mL), CTAB (0.6 g) and concentrated ammonia solution (1 g, 4.0 mL, 28 wt%) and was well dispersed. After dispersion, 0.4 g of tetraethyl orthosilicate (TEOS) was added dropwise and the reaction was allowed to proceed for 12 h under continuous mechanical stirring. The resulting product was washed with distilled water and ethanol (1:1) and the core–shell cobalt oxide mesoporous silica microspheres were dried at 50 C$^{\circ}$.

2.2.3. Synthesis of Co_3O_4 co-doped TiO_2 (Co_3O_4/TiO_2)

Equi-molar aqueous solutions of TiO_2 and cobalt nitrate hexahydrate were mixed together and basified with NH_4OH solution till pH reached above 10.0. This ensuing high basic solution was stirrer at 60.0 ^{0}C for overnight and the resulting product was washed with a mixture of distilled water and ethanol (1:1). The product was then dried at room temperature and further calcined at 400.0 ^{0}C for 5 hours.

2.2.4. Synthesis of Co_3O_4 co-doped Fe_2O_3 (Co_3O_4/Fe_2O_3)

Equal amount of Ferric's and cobalt's salts were accurately weighed and dissolve entirely in 100 mL distilled water at ambient temperature. The pH of the solution was adjusted to 11 by dropwise addition of freshly prepared 0.2 M NaOH solution under constant and vigorous stirring. After that the solution was kept at 60-70 °C for overnight with continuous stirring. Now decrease the temperature of the solution and centrifuged as to separate the precipitate at 2000 rpm. Discard the supernatant solution and washed the precipitate thrice with ethanol. The precipitate was dried in oven at 50-60 °C, grind and stored in a clean, dry and inert plastic vials.

2.2.5. Synthesis of core–shell zinc oxide silica nanoparticles ($ZnO@SiO_2$)

ZnO@SiO$_2$ nanoparticles were synthesized by the same sol–gel method as Co$_3$O$_4$@SiO$_2$. The aqueous dispersion of ZnO nanoparticles (0.2 g) was mixed with ethanol (80 ml), water (20 mL), 2 g tetraethyl orthosilicate (TEOS) and concentrated ammonia solution (6 mL, 28 wt%) in a conical flask and allowed to proceed for 12 h under a continuous stirring. The resulting product was washed with 1:1 mixture of distilled water and ethanol by drying the core shell of zinc silica nanoparticles at 50 C$^\circ$.

2.3. Characterization of nanomaterials

The morphology and average size of the as-grown Co$_3$O$_4$, Co$_3$O$_4$@SiO$_2$, Co$_3$O$_4$/TiO$_2$, Co$_3$O$_4$/Fe$_2$O$_3$, ZnO@SiO$_2$ were analyzed by field emission-scanning electron microscope (FESEM), JEOL (JSM-7600F, Japan). Energy dispersive X-rays spectrometry (EDS) of Co$_3$O$_4$@SiO$_2$ was carried out for the elemental analysis by using oxford-EDS system. The structure of Co$_3$O$_4$@SiO$_2$ was analyzed by ARL Service Powder Diffractometer, while FT-IR analysis was carried out by using Bruker (ALPHA, USA) in 4000-400 cm^{-1}.

2.4. Preparation of modified gold electrodes (AuE) for H$_2$O splitting

The surface of AuE was polished with alumina slurry (0.05 μM), and thoroughly rinsed with deionized water and ultra sonicated with pure deionized water and air dried. The slurry was made by properly mixing the nanomaterials (5 mg) with 5 μL of 0.01% nafion solution. Paste the slurry on AuWE and dried at room temperature. The current generated by catalyst was measured in aqueous KOH electrolytes, consisting of three electrodes, AuE coated with nanomaterial operating as working electrode, while Pt metal wire as the counter electrode, and Ag/AgCl as a reference electrode. All the three electrodes were dipped in a glass cell having KOH solution, and separated from each other at certain distance. To avoid any disruption during the

experiment, nitrogen gas was bubbled thoroughly to evacuate the glass cell. The current verses potential was measured at 50 mV/s sweep rate. Epsilon electrochemical workstation coupled with BAS*i Cell Stand* C3 was used for electrochemical studies. The measurements for water oxidation were carried out in aqueous KOH electrolytes at pH 13, 13.2, 13.3, 13.4, and 13.6.

3. Results and Discussions

3.1. *Structural characterization of nanoparticles*

In this study, we prepared five different nanomaterials such as Co_3O_4, $Co_3O_4@SiO_2$, Co_3O_4/TiO_2, Co_3O_4/Fe_2O_3, and $ZnO@SiO_2$. The FESEM was used to examine the morphology of the as grown nanomaterials as shown the images in Fig. 1. The FESEM images show that the prepared nanomatterials has grown in the form of particles except Co_3O_4/Fe_2O_3 which is a mixture of nanoparticles and fibers. The high magnified FESEM image of the nanomaterials, specifies that the particles grown with < 50 nm in diameter. The FESEM images clearly indicated that $Co_3O_4@SiO_2$ is mesophorous in nature and therefore might have larger surface area as compared to other nanomaterials. Surface area (SA) of $Co_3O_4@SiO_2$ was measured by using the N_2-sorption technique which was found to be 14 m^2/g. We explored all the nanomaterials as discussed above for the oxygen evolution reaction (OER), in which $Co_3O_4@SiO_2$, TiO_2/Co_3O_4, Co_3O_4, showed good catalytic activity. However it was found that among all the nanomaterials, $Co_3O_4@SiO_2$ showed excellent catalytic activity in water oxidation and this might be due to large surface area of $Co_3O_4@SiO_2$ which generally responsible for high catalytic activity in water oxidation. By viewing the efficient catalytic properties of $Co_3O_4@SiO_2$, we further characterized it by EDS, XRD and FTIR and selected for further detailed electrochemical analysis.

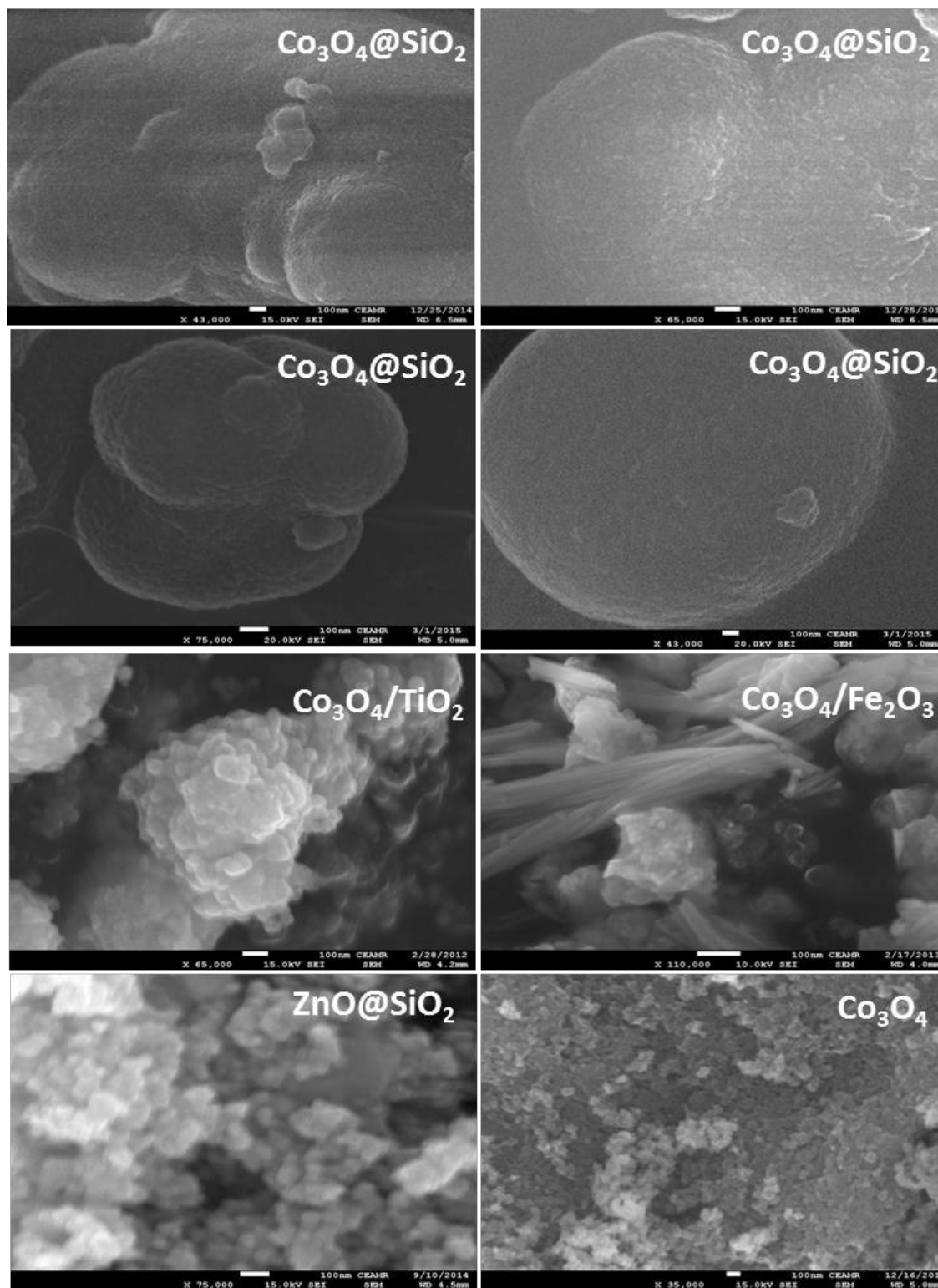**Fig. 1.** Typical low and high resolution FESEM images of Co_3O_4, $Co_3O_4@SiO_2$, Co_3O_4/TiO_2, Co_3O_4/Fe_2O_3, $ZnO@SiO_2$.

The morphology of $Co_3O_4@SiO_2$ was also examined by TEM (Fig. 2) which shows sphere like structures.

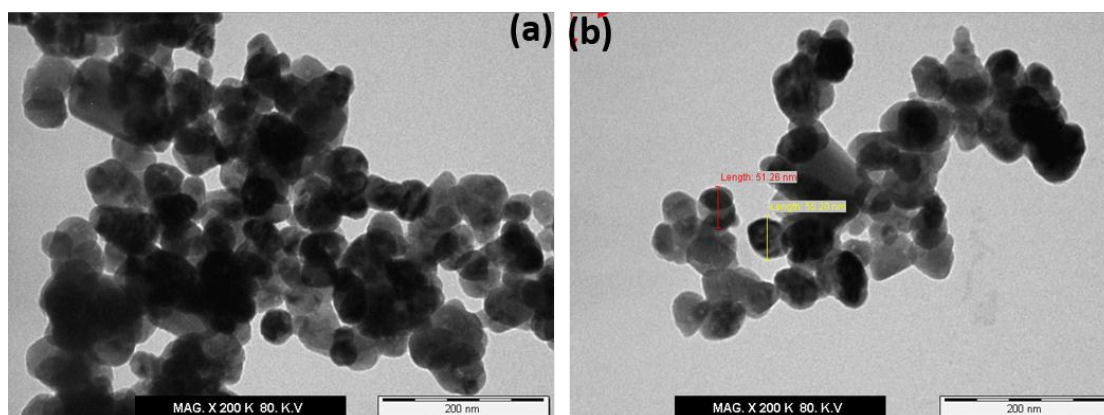**Fig. 2.** Typical TEM images of (a) $Co_3O_4@SiO_2$.

Further the composition of the synthesized $Co_3O_4@SiO_2$ was determined by EDS spectrum as shown in Fig. 3. The EDS spectrum of $Co_3O_4@SiO_2$ is showing peaks for O, Co, Si and C. These peaks confirm the formation of $Co_3O_4@SiO_2$, while the peak appeared for carbon is due to the surfactant used for the formation of $Co_3O_4@SiO_2$. Thus EDS confirmed that the as-grown nanoparticles were composed of cobalt, silicon, carbon and oxygen. It was further confirmed from the weight % compositions in EDS that Co and Si exist in 5 and 3 wt%, respectively. The EDS spectrum of Co_3O_4 has shown peaks for O and Co while peaks for O, Co and Ti were observed in Co_3O_4/TiO_2. Similarly, Co_3O_4/Fe_2O_3 and $ZnO@SiO_2$ samples displayed peaks related to O, Co, Fe and O, Zn and Si, respectively.

10

Element	Weight%	Atomic%
C K	60.97	70.88
O K	30.00	26.18
Si K	3.09	1.53
Co K	5.95	1.41
Totals	100.00	
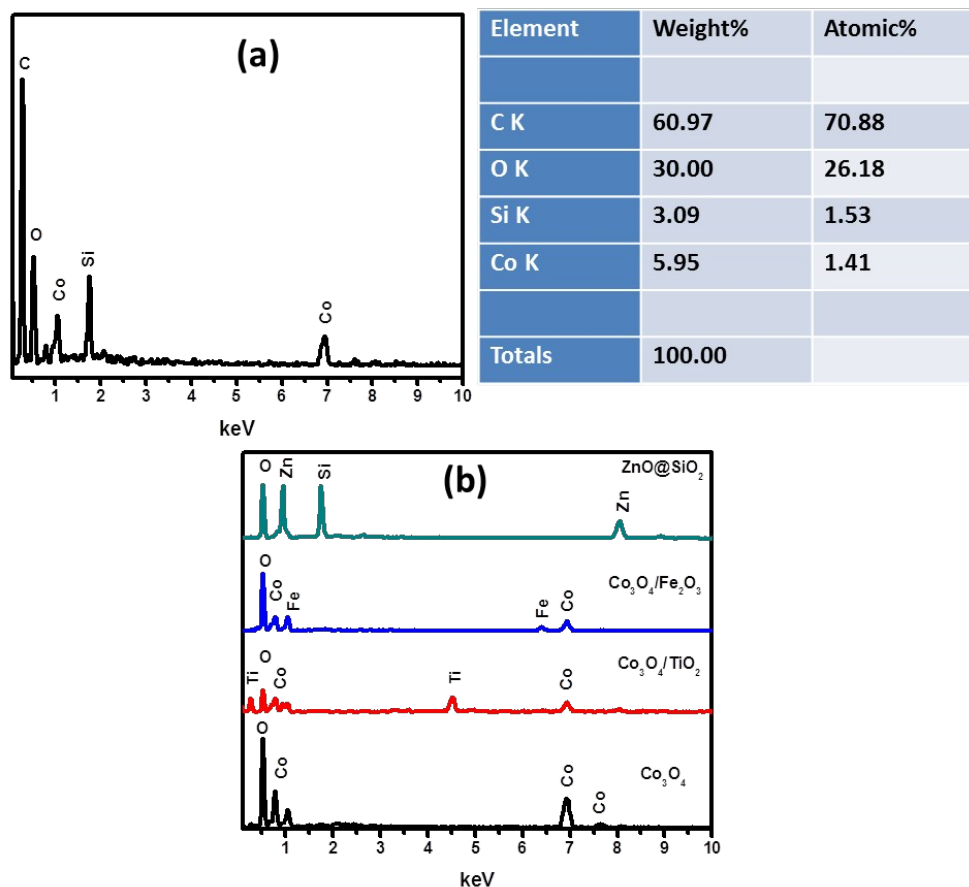
Fig. 3. Typical EDS spectrum of (a) $Co_3O_4@SiO_2$ and (b) Co_3O_4, Co_3O_4/TiO_2, Co_3O_4/Fe_2O_3, $ZnO@SiO_2$.

The structure of $Co_3O_4@SiO_2$ was characterized by XRD as shown in Fig. 4 (a). XRD spectrum exhibit a hallow peak along with well-defined crystalline peak. The hallow peak is attributed to the silica core shell while the sharp crystalline peaks appeared for Co_3O_4 in the XRD spectrum. The Co_3O_4 peaks exactly matched with JCPDS # 80-1536. The XRD patterns confirmed that the synthesized nanoparticles were composed of Co_3O_4 [21]. The Co_3O_4, Co_3O_4/TiO_2, Co_3O_4/Fe_2O_3, $ZnO@SiO_2$ is shown in Fig. 4(c). Co_3O_4 is showing peaks at 2θ of 20.4, 29.1, 37.3, 39.1, 50.9, 56.0, 59.8, 65.7 and 69.3 which reveal that cobalt oxide exist in tetragonal arrangement of Co_3O_4 [21]. Co_3O_4/TiO_2 is exhibiting peaks for Co_3O_4 and TiO_2 which suggest that cobalt oxide and titanium oxide exist in the doped material. The XRD data closely match the

literature [22]. Similarly, Co_3O_4/Fe_2O_3 is showing peaks for both Co_3O_4 and Fe_2O_3 and the results are in good agreement with the literature [21]. $ZnO@SiO_2$ presents peaks sequence wurtzite hexagonal ZnO nanoparticle [23].
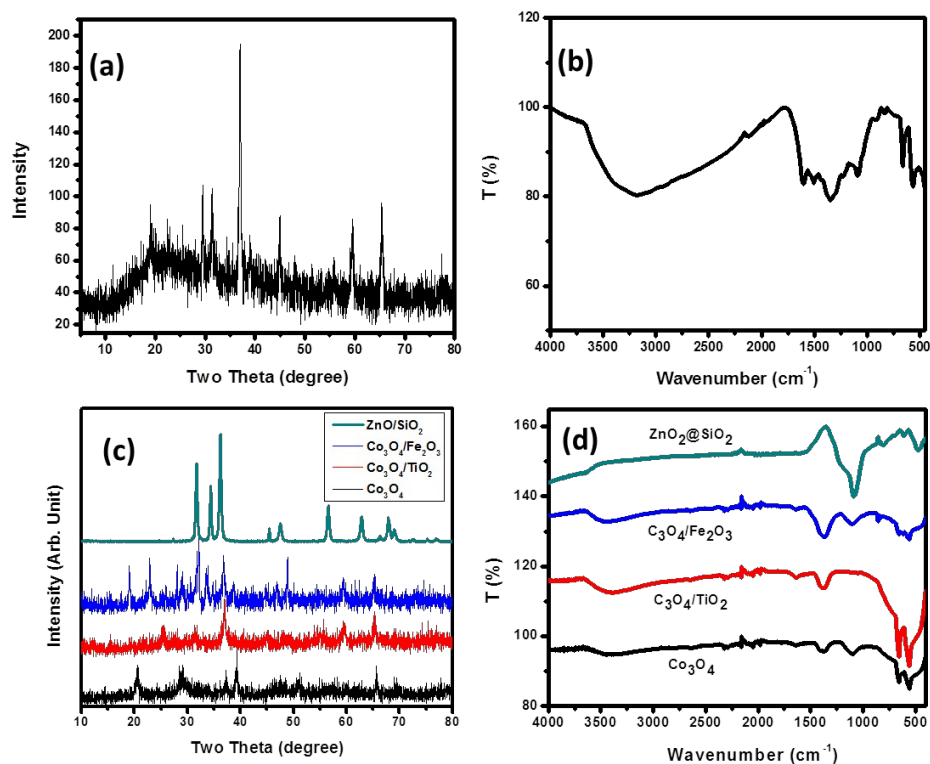

Fig. 4. Typical (a) XRD of $Co_3O_4@SiO_2$, (b) FTIR of $Co_3O_4@SiO_2$, (c) XRD of Co_3O_4, Co_3O_4/TiO_2, Co_3O_4/Fe_2O_3, $ZnO@SiO_2$ and (d) FTIR of Co_3O_4, Co_3O_4/TiO_2, Co_3O_4/Fe_2O_3, $ZnO@SiO_2$

FT-IR spectrum of $Co_3O_4@SiO_2$ is showing absorptions for various functional group at 567 (M=O), 667 (M-O-M, stretching), 1605 (O-H bending vibration) 3227 cm^{-1} (O-H stretching) and the other peaks in the range of 1086-1320 cm^{-1} are due to the presence of SiO_2. The CO_2 or CO_3^{-2} were absorbed due to the mesophorous nature of the nanomaterials and so appeared at 1330 cm^{-1}, as indicating in Fig. 4 (b). These data suggests that the synthesized nanomaterial is metal oxide based nanostructure [24]. The FTIR spectrum of the Co_3O_4, showed absorption at 567 cm^{-1} (M=O), and 655 cm^{-1} (M-O-M, stretching), while Co_3O_4/TiO_2 displayed absorptions at 1374 (CO_2 or CO_3^{-}

^{2}), 558 (M=O), and 655 cm^{-1} as shown in Fig. 4 (d). The absorption peak at 1374 cm^{-1} (CO$_2$ or CO$_3^{-2}$) and 558 cm^{-1} (M=O) were appeared in the FTIR spectrum of Co$_3$O$_4$/Fe$_2$O$_3$. Similarly the FTIR spectrum of ZnO@SiO$_2$ showed a prominent peak at 1084 cm^{-1}, confirmed the presence of SiO$_2$ in ZnO@SiO$_2$ along with a peak at 558 cm^{-1} (M=O) as shown in Fig. 4 (d) [21-24].

3.2. *Electrocatalytic performance of nanomaterials for H$_2$O oxidation*

Cobalt oxide is an efficient catalyst for oxygen evolution reaction in alkaline conditions. Therefore, we determined the electrocatalytic properties of cobalt oxide based nanoparticles in water splitting using alkaline conditions. Cobalt based nanomaterials such as Co$_3$O$_4$, Co$_3$O$_4$@SiO$_2$, Co$_3$O$_4$/TiO$_2$, Co$_3$O$_4$/Fe$_2$O$_3$, ZnO@SiO$_2$ were coated on the surface of AuE and evaluated for their water oxidation study in 0.1 M KOH aqueous solution (pH 13) by observing linear sweep voltammograms (LSVs) as shown in Fig. 5 (a,b). Among all nanomaterials, Co$_3$O$_4$@SiO$_2$ was found to be the most active electrocatalyst which play an important role in the process of oxygen evolution reaction in alkaline conditions. The linear sweep voltammogram of Co$_3$O$_4$@SiO$_2$ was also compared with bared AuE in Fig. 5 (c,d) and it was largely found that Co$_3$O$_4$@SiO$_2$ displaying higher catalytic activity toward OER in water oxidation as compared to bared AuE.

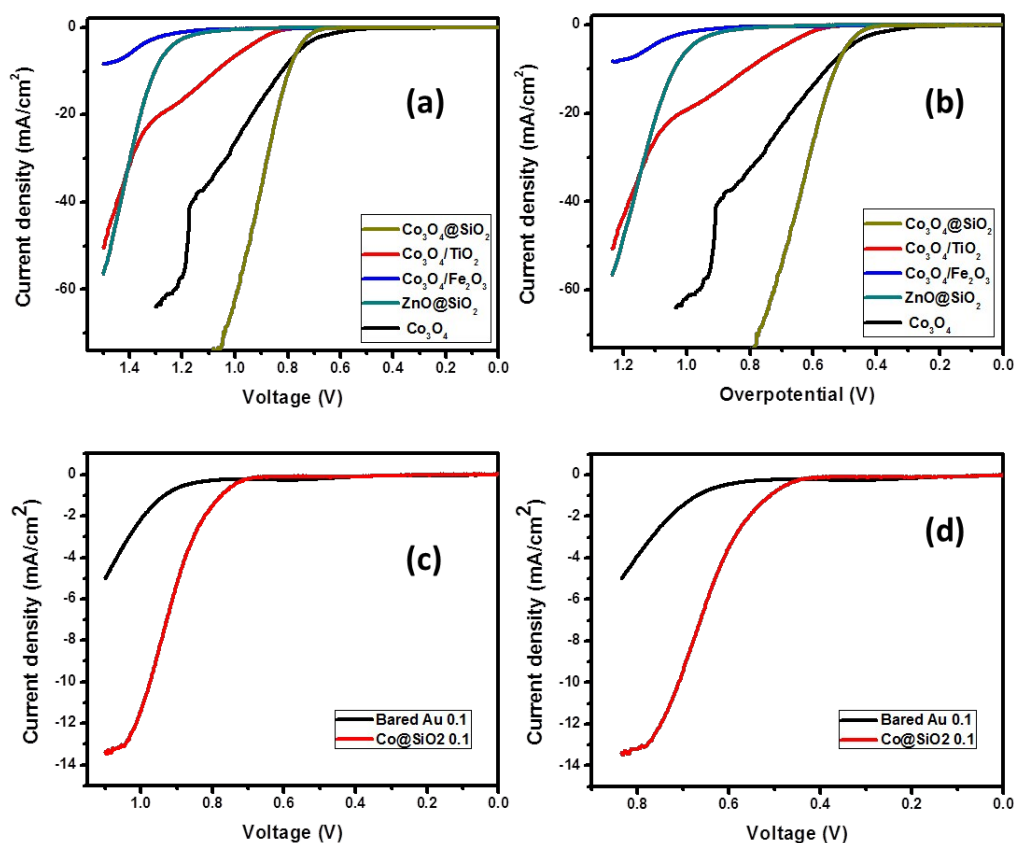**Fig. 5.** Linear sweep voltammograms of (a, b) Co_3O_4, $Co_3O_4@SiO_2$, Co_3O_4/TiO_2, Co_3O_4/Fe_2O_3, $ZnO@SiO_2$ and (c, d) comparison of $Co_3O_4@SiO_2$ linear sweep voltammogram with bared AuE in 0.3 M KOH solution.

By comparing the OER catalytic performance of $Co_3O_4@SiO_2$ with pure Co_3O_4 and other doped cobalt oxide such as Co_3O_4/TiO_2, Co_3O_4/Fe_2O_3, it was found that $Co_3O_4@SiO_2$ exhibit excellent performance in OER. At 1.0 V (overpotential 735 V versus Ag/AgCl) $Co_3O_4@SiO_2$ exhibited a current density of 63.0 $mAcm^{-2}$ in 0.1 M KOH solution. At the same condition, other nanomaterials such as Co_3O_4 and Co_3O_4/TiO_2 displayed current density (at 1.0 V) of 26.7 and 6.7 $mAcm^{-2}$, respectively while and Co_3O_4/Fe_2O_3 exhibited negligible current density. The $Co_3O_4@SiO_2$ showing low overpotential value of 529 mV at current density of 10 mA/cm^2 while the other nanomaterials exhibit higher overpotentials at same current density. Further

to assess the effect of silica on the water oxidation performance, the $Co_3O_4@SiO_2$ was compared with $ZnO@SiO_2$. $ZnO@SiO_2$ is showing very low current even at very high overpotential which suggests that silica is not responsible for high catalytic performance but the mesopourus nature of $Co_3O_4@SiO_2$ might be important in water oxidation.

At pH 13 the standard potential for the anode was $E°_{OH–/O2} = 0.463$ V vs. standard hydrogen electrode (SHE), which corresponds to 0.265 V vs. the Ag/AgCl reference electrode, used for the all overpotential measurements [25, 17]. The overpotentials of bared electrode and nanomaterials (Co_3O_4, $Co_3O_4@SiO_2$, Co_3O_4/TiO_2, Co_3O_4/Fe_2O_3, $ZnO@SiO_2$) were observed at a specified current density (5 mA/cm^2 and 10 mA/cm^2), while current densities of these nanoparticles vs. reference Ag/AgCl was observed at 1V as shown in Table-1. We observed that at a given potential $Co_3O_4@SiO_2$ indicated the highest current density as compared to bared electrode as well as from all other nanomaterials. $Co_3O_4@SiO_2$ exhibited a current density of 10 mA/cm^2 at 794 mV (vs. Ag/AgCl), respectively, corresponding to an overpotential of 529 mV. Similarly, current densities of 20 and 40 mA/cm^2 were obtained at 838 and 912 mV (vs. Ag/AgCl) for $Co_3O_4@SiO_2$, respectively, which correspond to an overpotentials of 573 and 647 mV, respectively, displaying an excellent OER activity of $Co_3O_4@SiO_2$ nanoparticles. To obtain a current density of 10, 20 and 40 mAcm^{-2} it was found that by using alkaline KOH solution of pH-13, $Co_3O_4@SiO_2$ needed only an overpotentials of 529, 573 and 647 mV, respectively.

15

Table 1. Overpotential (at 10, 20 and 40 mA/cm^2) and current density (at 1.0 V vs. Ag/AgCl) of Co$_3$O$_4$, Co$_3$O$_4$@SiO$_2$, Co$_3$O$_4$/TiO2, Co$_3$O$_4$/Fe$_2$O$_3$, ZnO@SiO$_2$ (0.3 M KOH).

Catalyst	Overpotential (mV) at 10 mA/cm^2	Overpotential (mV) at 20 mA/cm^2	Overpotential (mV) at 40 mA/cm^2	Current density (mA/cm^2) at 1 V (vs. Ag/AgCl)
Co$_3$O$_4$	560	678	910	26.7
Co$_3$O$_4$@SiO$_2$	529	573	647	63.2
Co$_3$O$_4$/TiO$_2$	812	1026	1185	6.7
Co$_3$O$_4$/Fe$_2$O$_3$	-	-	-	0.4
ZnO@SiO$_2$	1036	1092	1169	0.7

For an electrochemical reactions the type of electrolyte, pH and concentration of electrolyte are the key parameters in water splitting [17]. Generally in case of basic metal oxides like Co$_3$O$_4$, concentrated alkali solution is used as an electrolyte for oxygen evolution. A series of different concentration of KOH solutions was prepared to check the electrocatalytic activity of the Co$_3$O$_4$@SiO$_2$ as shown in Fig. 6 (a, b). The effect of different concentration of alkaline KOH solution is indicated in Table-2, which shows the direct proportionality of current densities with the concentration of alkaline solution. The current density for Co$_3$O$_4$@SiO$_2$ at 1 V (vs. Ag/AgCl) is 11.5 mA/cm^2 using pH 13. By increasing the pH of the solution from 13 to 13.6 the current density was also increased from11.5 mA/cm^2 to 63.2 mA/cm^2 at 1V (vs. Ag/AgCl). In order to compare the catalytic activities at different pH, the thermodynamic potentials and over potentials of the catalyst were calculated at particular current densities. At different concentration (pH 13, 13.2, 13.3, 13.4 and 13.6), the overpotentials of 715,

16

593, 552, 529, and 529 mV were measured at 10 mA/cm^2 current density, respectively as shown in Table-2. It was concluded that the oxidative catalytic activity of $Co_3O_4@SiO_2$ was increased by increasing the OH$^-$ ions concentration in the electrolyte.
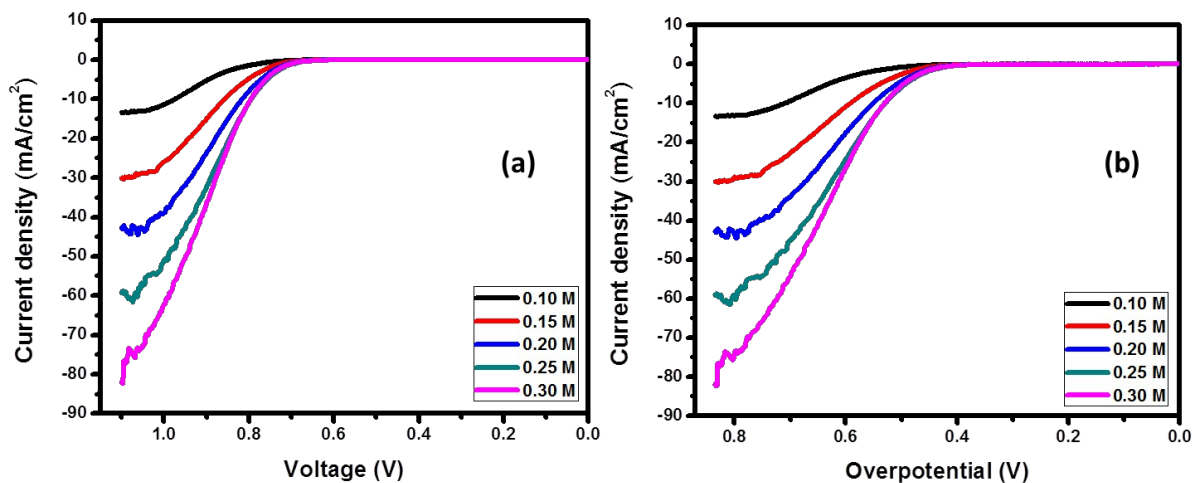

Fig. 6. Linear sweep voltammograms and cyclic voltammograms of $Co_3O_4@SiO_2$ in different pH of KOH solution.

Table 2. Overpotential (at 10, 20 and 40 mA/cm^2) and current density (at 1.0 V vs. Ag/AgCl) of $Co_3O_4@SiO_2$ in KOH electrolyte of different pH.

Catalyst $Co_3O_4@SiO_2$	Overpotential (mV) at 10 mA/cm^2	Overpotential (mV) at 20 mA/cm^2	Overpotential (mV) at 40 mA/cm^2	Current density (mA/cm^2) at 1 V (vs. Ag/AgCl)
pH 13	715	-	-	11.5
pH 13.2	593	680	-	26.2
pH 13.3	552	616	758	38.8
pH 13.4	529	585	670	52.1
pH 13.6	529	575	647	63.2

The catalysis activity of $Co_3O_4@SiO_2$ was scrutinized by Tafel slope values. Tafel plots showed the result of cobalt based composite nanoparticles at different concentration of alkaline KOH indicated in Fig. 7. The linear portions of the Tafel plots are fitted to the Tafel equation *i.e.* $\eta = b\log(j/j_o)$ where η represent overpotential, j denotes the current density, j_o is the exchange current density, b is the Tafel slope [6]. The catalyst-modified electrode is an intrinsic property in Tafel slope indicated the rate-limiting step for the OER. Tafel slope of $Co_3O_4@SiO_2$ was found to be 151.3 mV dec^{-1} at pH 13 while Tafel slope of 127.5, 111.3, 107.9 and 107.7 was observed at pH 13.2, 13.3, 13.4, and 13.6 mV dec^{-1} as shown in Fig. 7. This suggests the apparently similar kinetics of the OER activity in different concentrations of KOH solution. These results stipulate that cobalt based composite nanoparticles indicated higher OER catalytic activity at higher pH. As anticipated, the cobalt based composite

18

nanoparticles catalyst gives the insignificant Tafel slope of 107.7 mV dec^{-1} in 0.3 M
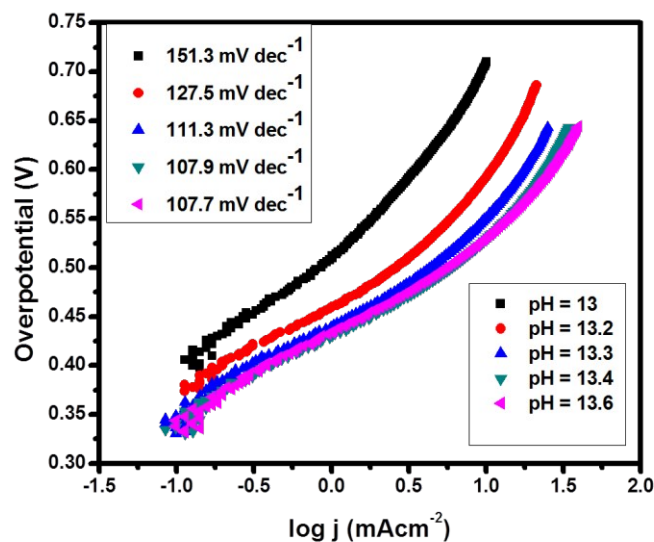
KOH solution.

Fig. 7. Tafel plots of $Co_3O_4@SiO_2$ at different pH.

The stability of catalyst is very important for the long term use of a catalyst in

OER process [26]. Therefore the stability and durability of $Co_3O_4@SiO_2$ was studied

by measuring OER activities many times with one minute intervals using LSV (Fig.

8). After many scans, the OER activity of $Co_3O_4@SiO_2$ did not change any

deactivation in activity of $Co_3O_4@SiO_2$. The superior stability and durability of

$Co_3O_4@SiO_2$ might be due to SiO_2 which maintain the original structure even after
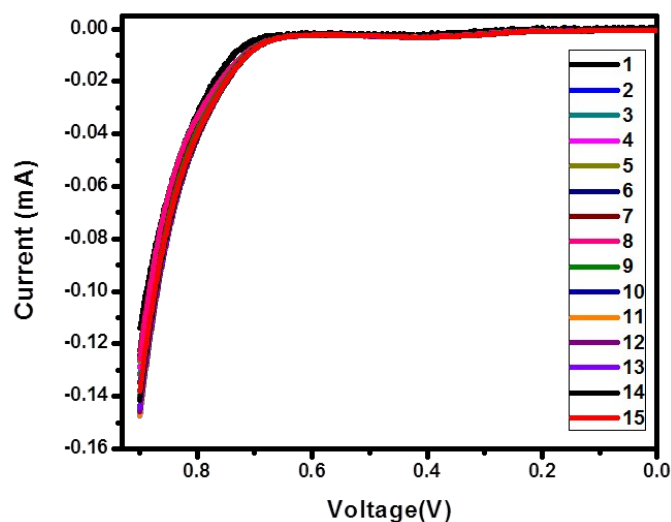
long stability and durability test [26].

Fig. 8. Different scans of linear sweep voltammograms of $Co_3O_4@SiO_2$.

Now a day Co-based OER catalysts find interest in water oxidation (Fig. 9), yet attempted is being continuous for the search of better cobalt-based catalysts for electrochemical OER studies both in basic and in neutral electrolyte solutions due to their low overpotential value [16]. It is difficult to compare directly the OER activity presented in this paper with previous results, because of different experimental conditions. However, under some similar experimental conditions obtained [13-19], comparisons with some recent OER results with the data presented in this paper, indicating the superior catalytic activity of the $Co_3O_4@SiO_2$ catalyst. Further the Tafel slope and overpotential values of $Co_3O_4@SiO_2$ catalysts at 10 $mAcm^{-2}$ were considerably less than the literature using the same 0.1 M KOH electrolyte as summarized in Table 3 [27-31].
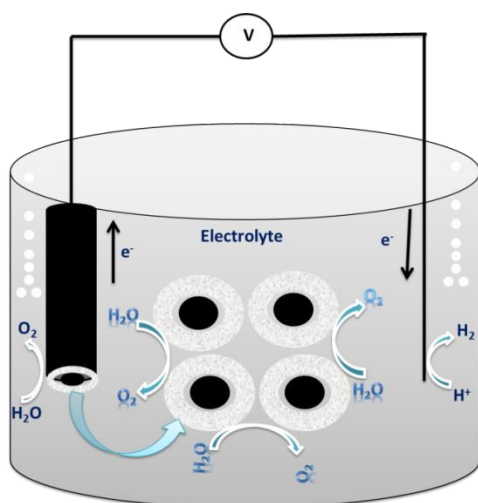
Fig. 9. Schematic view of water splitting mechanism using $Co_3O_4@SiO_2$ as electrocatalyst.

Table 3. Tafel slope comparison of $Co_3O_4@SiO_2$ with literature.

Catalyst	Electrolyte	Tafel Slope (mV dec^{-1})	References
Co_3O_4/SWNTs	1.0 M KOH	104	[27]
G-Mn-NiCo	0.1 M KOH	371.3	[28]
PNG-NiCo	0.1 M KOH	156	[29]
Ni-NG	0.1 M KOH	188.6	[30]
Ni_3S_2/Ni	0.1 M KOH	159.3	[31]
$Co_3O_4@SiO_2$	0.1 M KOH	151.3	This work
$Co_3O_4@SiO_2$	0.3 M KOH	107.7	This work

4. Conclusions

We evaluate the potential application of electrocatalytic activity of various cobalt based nanoparticles (Co_3O_4, $Co_3O_4@SiO_2$, Co_3O_4/TiO_2, Co_3O_4/Fe_2O_3, $ZnO@SiO_2$), in water oxidation which provide good catalytic activity to Co_3O_4, $Co_3O_4@SiO_2$, and Co_3O_4/TiO_2. However among Co_3O_4, $Co_3O_4@SiO_2$, Co_3O_4/TiO_2 the super catalytic performance in electrochemical water splitting was shown by $Co_3O_4@SiO_2$. This superior catalytic performance was attributed to the mesophorous nature of $Co_3O_4@SiO_2$, which increases the surface area and could possibly expose the active sites of the catalyst, which further elevated the electronic conductivity, oxidizing capacity, the affinity among the OH ion of the catalyst. The mesophorous nature of $Co_3O_4@SiO_2$ also increases surface and smooth mass transports which ultimately reduce the overpotential required for oxygen evolution reaction and leads to superior oxygen evolution activity and higher catalytic performance of $Co_3O_4@SiO_2$.

References

1. S. Solomon, D. Qin, M. Manning, Z. Chen, M. Marquis, K.B. Averyt, M. Tignor, H.L. Miller (Eds.) Cambridge University Press, Cambridge, United Kindom and New York, NY, USA, **2007**.

2. K. Akihiko, M. Yugo, *Chem. Soc. Rev*., 38, (**2009**), 253-278.

3. W. Wang, Q. Zhao, J. Dong, J. Li., *Int. J. hydrogen energy,* 36, (**2011**), 7374 - 7380.

4. C.J. Winter, *Int. J. Hydrogen Energy*, 34, (**2009**), 51-52.

5. J. Messinger, *Chem. Sus. Chem*., 2, (**2009**), 47-8.

6. T. Kodama, N. Gokon, *Chem. Rev*., 107, (**2007**), 4048-77.

7. A. Steinfeld, *Solar energy*, 78, (**2004**), 603-15.

8. N. Armaroli, V. Balzani, *Anew. Chem. Int. Ed. Engl*., 46 (**2007**) 52.

9. D.J. Nocera, *Inorg. Chem*., 48, (**2009**), 10001-17.

10. M.W. Kanan, D.J. Nocera, *Science*, 321, (**2008**), 1072-1075.

11. G. Pushpavanam, S. Pushpavanam, *Int. J. Hydrogen Energy*, 27, (**2002**), 627-33.

12. N.V. Krstaji, V.D. Jovi, L. Gaji, Krstai, B.M. Jovi, A.L. Antozzi, G.N. Martell, *Int. J. Hydrogen Energy*, 33, (**2008**), 3676-87.

13. P.C. Chen, Y.M. Chang, P.W. Wu, Y.F. Chiu, *Int. J. Hydrogen Energy*, 34, (**2009**), 6596-602.

14. F.A. Frame, R.L. Townsend, E.M. Chamousis, T. Sabio, N.D. Dittrich, Browning *et al J. Am. Chem. Soc.*, 133, (**2011**), 7264-7267.

15. Y. Surendranath, M. Dinca, D.G. Nocera, *J. Am. Chem. Soc*., 131, (**2009**), 2615-20.

16. A.J. Bard, M.A. Fox, *Acc. Chem. Res*., 28, (**1995**), 141-145.

17. M.W. Kanan, Y. Surendranath, D.G. Nocera, *Chem. Soc. Rev*., 38, (**2009**), 109-14.

18. D.A. Lutterman, Y. Surendranath, D.G. Nocera, *J. Am. Chem. Soc*., 131, (**2009**), 3838-9.

19. Y. Liang, Y. Li., H. Wang, J. Zhou, J. Wang, T. Regier, H. Dai, *Nat Mater.,* 10, (**2011**), 780-786.

20. Z. Sun, Q. Yue, Y. Liu, J. Wei, B. Li, S. Kaliaguine, Y. Deng, Z. Wu, D. Zhao, *J. Mater. Chem. A*., 2, (**2014**), 18322–18328.

21. S.A.B. Asif, S.B. Khan, A.M. Asiri, *Nanoscale Res. Lett.,* 9, (**2014**), 510.

22. S.B. Khan, M.M. Rahman, A.M. Asiri, H.M. Marwani, S.M. Bawaked, K.A. Alamry, *NJC*., 37, (**2013**), 2888-2893.

23. S.B. Khan, M. Faisal, M.M. Rahman, A. Jamal, *Talanta*, 85, (**2011**), 943–949.

24. S.B. Khan, M. Faisal, M.M. Rahman, A. Jamal, *Sci. Tot. Environ*., 409, (**2011**), 2987-2992.

25. H. Tuysuz, Y.J. Hwang, S.B. Khan, A.M. Asiri, P.D. Yang, *Nano Res*., 6, (**2013**), 47 -54.

26. X. Lu, Y. H. Ng, C. Zhao, *Chem. Sus. Chem.,* 7, (**2014**), 82–86.

27. J. Wu, Y. Xue, X. Yan, W. Yan, Q. Cheng, Y. Xie, *Nano Res*., 5, (**2012**), 521-530.

28. S. Chen, J. Duan, W. Han, S. Qiao, *Chem. Commun*., 50, (**2014**), 207-209.

29. S. Chen, S. Qiao, *ACS Nano*., 7, (**2013**), 10190-10196.

30. S. Chen, J. Duan, J. Ran, M. Jaroniec, S. Qiao, *Energy Environ. Sci.,* 6, (**2013**), 3693–3699.

31. W. Zhou, X. Wu, X. Cao, X. Huang, C. Tan, J. Tian, H. Liu, J. Wang, H. Zhang, *Energy Environ. Sci.,* 6, (**2013**), 2921-2924.